Electronic Supplementary Information

4f-2p-3d orbital overlap in metal-organic framework-derived CeO_2/CeCo-LDH heterostructure promotes water oxidation

Priyanka Maurya[a], Toufik Ansari[a], Arindam Indra[a*]

[a]Department of Chemistry, Indian Institute of Technology (BHU), Varanasi-221005, U.P, India.

E- mail: arindam.chy@iitbhu.ac.in

Chemicals

Cobalt chloride hexahydrate was purchased from Sigma Aldrich (99.9%). Urea (99.5%) and ammonium fluoride (98%) were bought from SRL. Cerium nitrate nonahydrate was purchased from SRL. All chemicals were used without any further purification. Nickel foam was purchased from AXYS technology. Double distilled water was used for all the experiments and electrochemical measurements.

Instruments

The crystallinity and phase identification of the synthesized catalysts were confirmed by room-temperature X-ray diffraction (Rigaku Miniflex 600) using Cu-K alpha radiation (1.54 Å).

The IR spectra were recorded with the Nicolet iS5 FTIR spectrometer in attenuated total reflection (ATR) mode in the range between 400- 4000 cm^{-1}.

The XPS spectra have been measured using a Thermo Fisher Scientific instrument with Al K-alpha radiation operated at 150 W to investigate the chemical state of the materials.

Microstructure and compositional analyses of the prepared materials were examined with the help of Field emission scanning electron microscopy (Nova Nano SEM 450) equipped with an EDS System, and the interlayer d-spacing of the synthesized catalysts was obtained by taking HR-TEM images (FEI TECNAI G2 20 TWIN) operated at 300 kV.

Activation of nickel foam (NF)[S1]

Nickel foam was cut into pieces (size; 1 cm x 2 cm) and treated with 3.0 M HCl under ultrasonication to remove the oxide layer. After treatment with HCl, nickel foam pieces were washed with water and ethanol repeatedly. The obtained activated nickel foam was dried in an air oven for 12 h at 50 ^{O}C for further use.

Synthesis of cobalt hydroxide carbonate template on nickel foam (Co-HC@NF)[S2]

The precursor compounds $CoCl_2.6H_2O$ (2 mmol) and urea (10 mmol) were dissolved in 12 mL of deionized water followed by the addition of NH_4F (4 mmol). The reaction mixture was stirred at room temperature for 30 minutes and transferred into a 50 Teflon cup (volume: 50 mL) and a piece of activated nickel foam was kept vertically into the solution so that only 1 cm^2 area of nickel foam was dipped in the solution. The autoclave was sealed and kept in a preheated electric oven for 5 h. After the natural cooling, Co-HC deposited nickel foam was taken out and washed with water followed by washing with ethanol. Washed CoHC@NF was dried at 50 ^{O}C for overnight.

Synthesis of ZIF-67@NF[S3]

In a 15 mL of glass vial, 5 mmol of 2-methyl imidazole (2MeIM) was dissolved in 5 mL methanol. Co-HC@NF was immersed vertically in the solution of 2MeIM. Afterward, the glass vial was covered and kept at room temperature for 12 h. After completion of the reaction, purple-colored ZIF-67 was deposited on nickel foam. The ZIF-67@NF was washed with methanol several times to remove extra 2-MeIM. ZIF-67@NF was dried at 50 ^{O}C for 12 h.

Synthesis of CeCo-2[S4]

A clear solution of $Ce(NO_3)_3.6H_2O$ (0.2 mmol) was obtained by dissolving it into 12 mL of the mixed solution of iso-propanol and ethylene glycol (8:2). The obtained clear solution was poured into a Teflon-lined autoclave. After that, ZIF-67@NF was vertically placed into the reaction mixture, and the autoclave was sealed. The sealed

autoclave was kept in an electric oven for 5 h at 120 ^{O}C. After 5 h, the reaction mixture was allowed to cool naturally to room temperature. Afterthat, CeCo-2 deposited nickel foam was dried at 60 ^{O}C for overnight. Similarly, CeCo-1 and CeCo-3 were obtained by changing the amount of $Ce(NO_3)_3.6H_2O$ (see Table S1).

Synthesis of CeO_2+Co-LDH@NF[S4]

The CeO_2+Co-LDH@NF was prepared by using Co-LDH as a precursor. First, 0.2 mmol of $Ce(NO_3)_3.6H_2O$ was dissolved in 12 mL of a mixed solution of iso-propanol and ethylene glycol (8:2). After that reaction was transferred into 50 mL Teflon-lined autoclave. The film of Co-LDH was vertically immersed and the autoclave was sealed. The sealed autoclave was kept in an electric oven at 120 ^{O}C for 5h. After completion of the reaction, the reaction mixture was allowed to cool down to ambient temperature. The CeO_2+Co-LDH@NF catalyst was dried at 60 ^{O}C overnight.

Synthesis of CeCo-LDH

The CeCo-LDH catalyst was prepared by immersing ZIF-67@NF in a 15 mL vial containing 5 mL solution of Ce(III) salt in isopropanol: ethylene glycol (8:2). Reaction mixture was kept at room temperature for 10 h. After completing the reaction time period, obtained catalyst was washed with isopropanol and dried at 60 ^{O}C for overnight.

Table S1: Details of the catalysts

Catalyst	Precursor	Synthesis conditions
Co-LDH	ZIF-67@NF	$CoCl_2.6H_2O$ (0.2 mmol)
CeCo-1	ZIF-67@NF	$Ce(NO_3)_3.6H_2O$ (0.1 mmol)
CeCo-2	ZIF-67@NF	$Ce(NO_3)_3.6H_2O$ (0.2 mmol)
CeCo-3	ZIF-67@NF	$Ce(NO_3)_3.6H_2O$ (0.3 mmol)
CeCo-LDH	ZIF-67@NF	$Ce(NO_3)_3.6H_2O$ (0.2 mmol), at room temperature
CeO_2+Co-LDH	Co-LDH@NF	$Ce(NO_3)_3.6H_2O$ (0.2 mmol)

Loading of RuO_2 on NF

3.5 mg RuO_2 was dispersed in 50 µL Nafion solution in ethanol-H_2O and dropcast on NF, dried in an air oven at 50 ^{O}C.

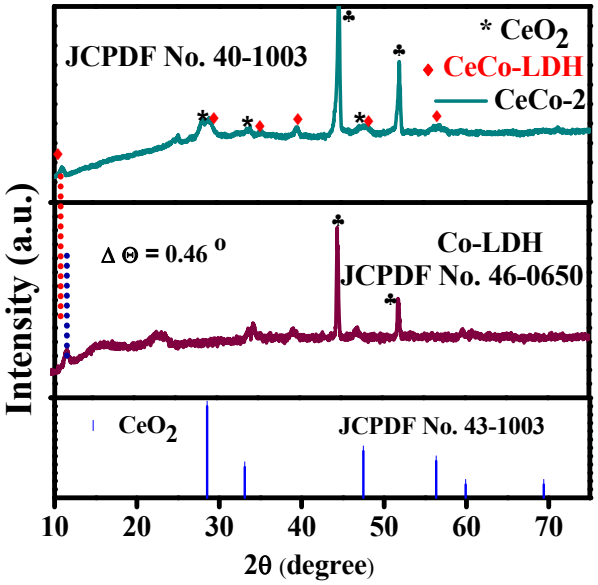

Figure S1. (Top) The powder X-ray diffraction pattern of CeCo-2 shows two distinct sets of peaks, confirming the presence of two phases. Peaks labeled with * correspond to CeO_2, while peaks marked with ♦ indicate CeCo-LDH. Additionally, ♣ marks denote the presence of nickel foam. The peaks obtained at 28.5°, 33.5°, 47.24°, and 56.5°, belong to (111), (200), (220), (311), and (222), planes of CeO_2 structure (JCPDS 34-0394) and the peaks at 10.92°, 34.9°, 39.29°, and 47.8°, were attributed to (003), (012), (015), and (018), planes of the CeCo-LDH (JCPDS 40-0215).[S5-S6]

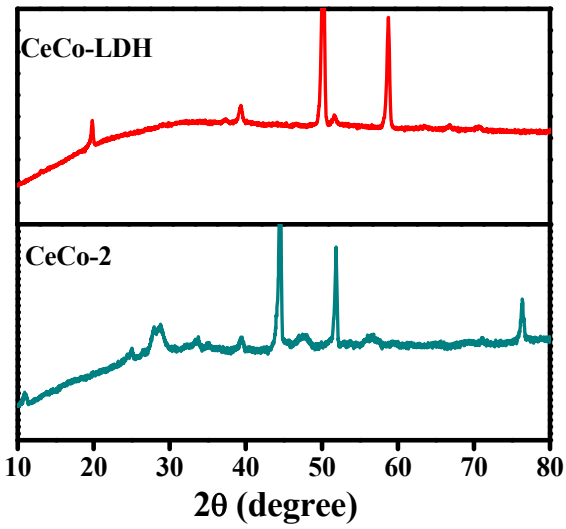

Figure S2. The powder X-ray diffraction pattern of CeCo-2 and CeCo-LDH.

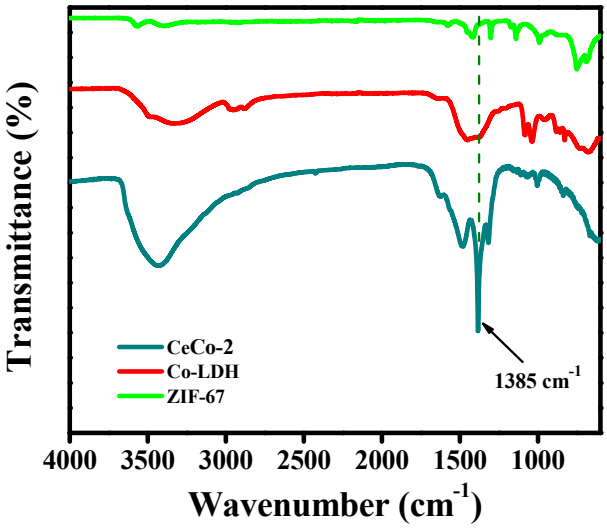

Figure S3. Fourier transformed infrared (FTIR) spectra of ZIF-67, Co-LDH and CeCo-2. Peak obtained at 1385 cm^{-1} confirms the presence of intercalated carbonate anion between the layers of Ce-Co-LDH.

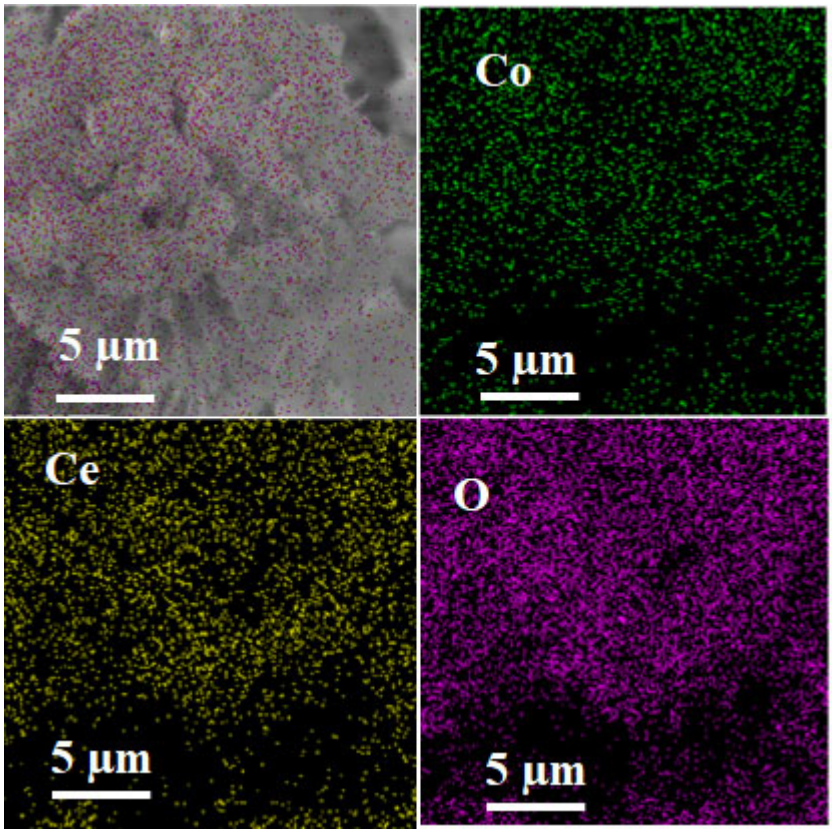

Figure S4. Elemental mapping of CeCo-2 showing the distribution of elements Ce, Co, C, and O.

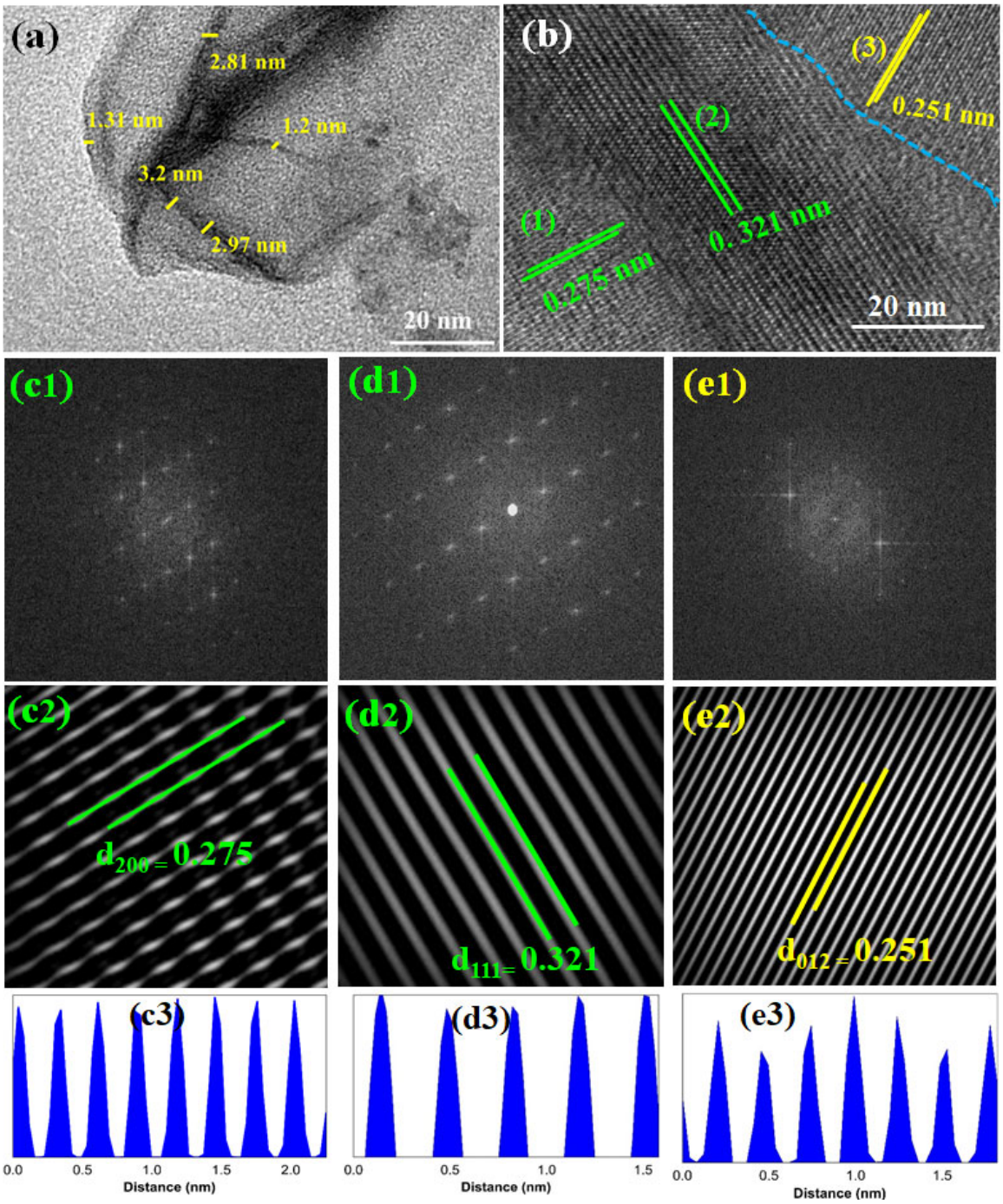

Figure S5. (a) The thickness of vertically grown CeCo-2 nanosheets. (b) HRTEM image of CeCo-2, (c1)-(e1) FFT of the areas (1), (2), and (3) in the figure (b), respectively. (c2)-(e2) The corresponding inverse FFT images of (c1)-(e1), respectively. (c3)-(e3)The contrast intensity profiles corresponding to the figures (c2)-(e2) showing the lattice parameters.

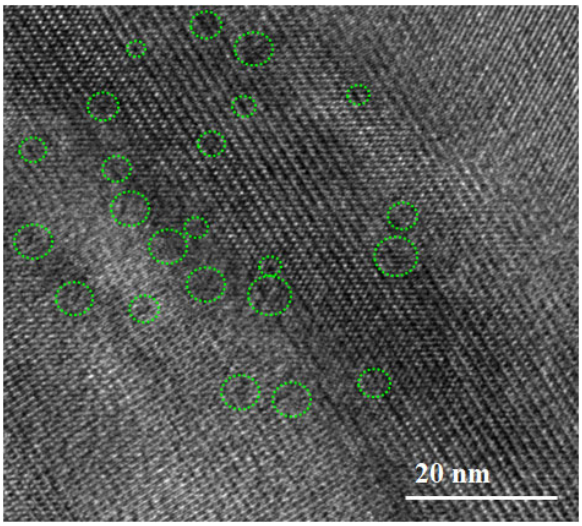

Figure S6. HRTEM image showing the defect rich sites (green circle) in CeO_2 of CeCo-2.

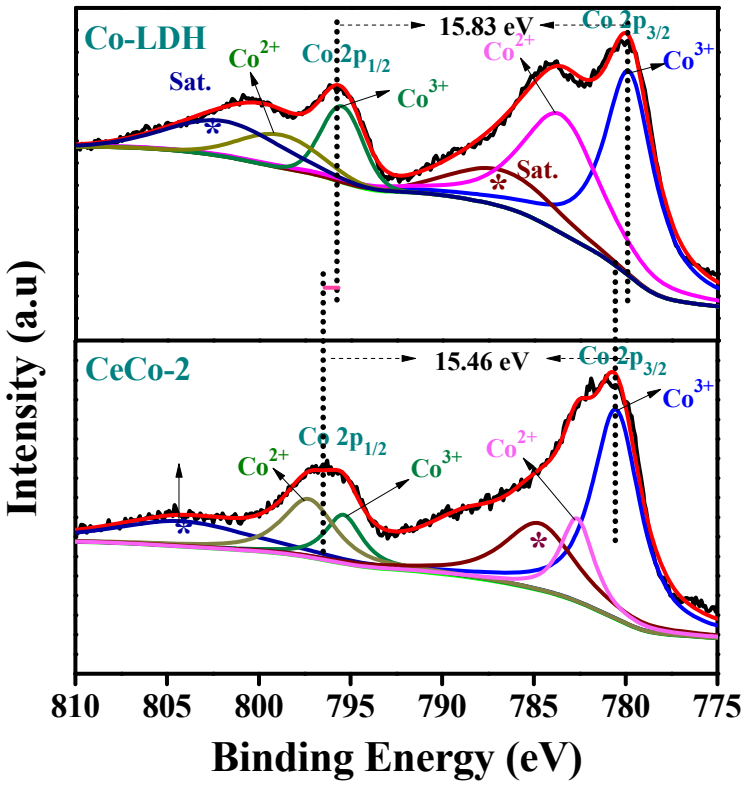

Figure S7. Co 2p XPS of Co-LDH is compared with that of CeCo-2. The incorporation of Ce in Co-LDH resulted in a significant modulation of the electronic structure as reflected in the shifting of the $Co2p_{3/2}$ to the higher binding energy. The spin-orbit spacing value is also decreased after the Ce incorporation in Co-LDH. The ratio of Co^{III}/Co^{II} amount in CeCo-2 was determined to be 1.86 by peak area integration. This value clearly showed that the incorporation of Ce^{III} and Ce^{IV} increased the amount of Co^{III} over Co^{II} in CeCo-2 compared to Co-LDH (ratio of Co^{III}/Co^{II} = 1.16). The satellite peaks for Co^{II} have also been detected in the Co 2p XPS of CeCo-2.The Co 2p XPS data was taken from the reference S5 with the permission from Royal Society of Chemistry and the figures were redrawn using the data.

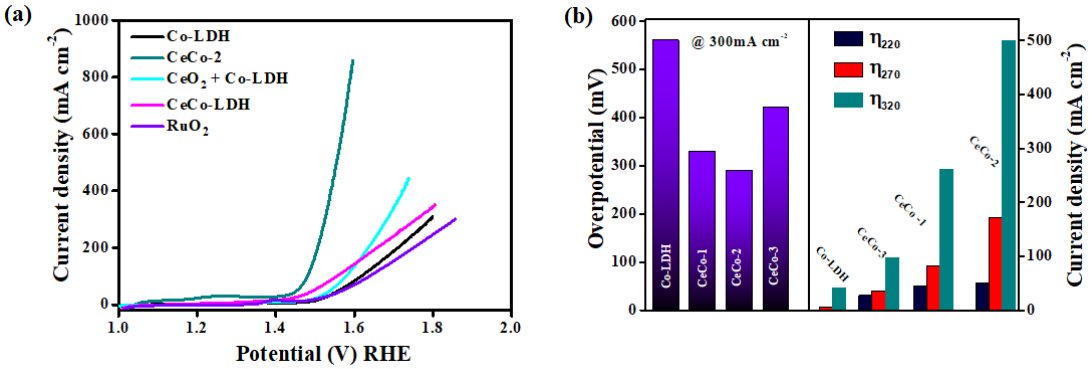

Figure S8. (a) LSV profiles for OER of the synthesized catalysts and benchmark catalyst RuO_2 showing the superior activity of CeCo-2, (b) comparative plots of overpotentials and current density for the different catalysts showing the best activity for CeCo-2.

Table S2. The OER activities of reported electrocatalysts compared with CeCo-2.

Entry	Catalyst	Current density (mA cm^{-2})	Overpotential	Reference
Co-based LDHs				
1	$V_{0.3}$-CoFe-LDH	10	240	S7
2	CoFeV LDH/NF	10	242	S8
3	$Co_{0.4}Fe_{0.6}$LDH/g-CN_x	10	270	S9
4	NiCoV-LDH	10	280	S10
5	Cr-CoFe-LDHs/NF	10	238	S11
ZIF-67-derived catalysts				
6	FeCo-LDH@$Co(OH)_2$	10	230	S12
7	NiFe-LDH/Co-NC-2	10	282	S13
8	NiFeCo-LDH/CF	10	249	S14
9	$Fe_{0.4}$Co-LDH@NF	20	190	S5
Ce-based catalysts				
10	**CeCo-2**	**500**	**320**	**This work**
11	FeOOH/CeO_2 HLNTs	17.6	250	S15
12	CeO_2/$Co(OH)_2$	10	250	S16
13	Ni_4Ce_1@CP	10	410	S17
14	Co_3O_4/CeO_2 NHs	10	270	S18
15	NiCoCe-LDH/CNT	10	236	S19
16	Ce-CoFe LDH	10	370	S20
17	CoO_x(Ce)	10	261	S21
18	$CoSe_2$/CeO_2	10	288	S22
19	Se-doped Co_3O_4@CeO_2	50	293	S23
20	Ce-NiFe-LDH/CNT	10	227	S24
21	CeO_x/CoS	10	269	S25
22	Co/Ce Ni_3S_2@NF	10	286	S26
23	CeO_2-Co_2O_3@NF	50	334	S27

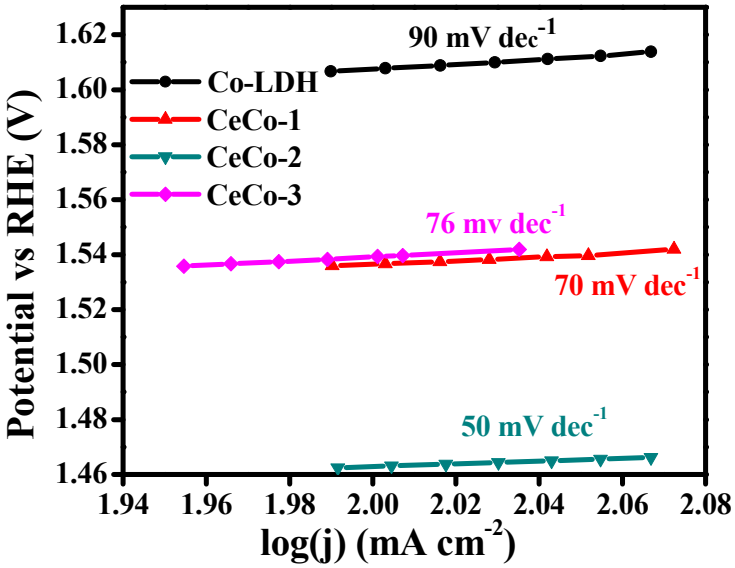

Figure S9. Tafel plots for the oxygen evolution reaction with CeCo-2 compared with other catalysts. The lowest Tafel slope for CeCo-2 suggests the fastest OER kinetics.

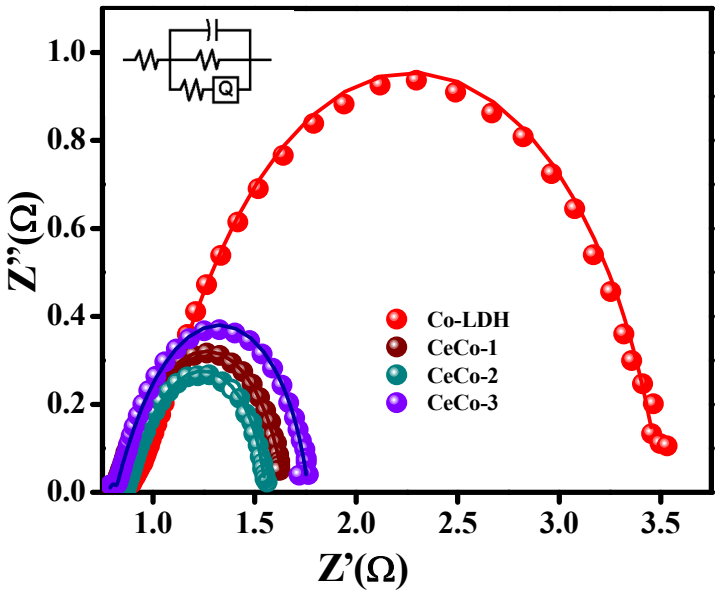

Figure S10. Nyquist plots for the CeCo-2, Co-LDH, CeCo-1, and CeCo-3, showing the lowest charge transfer resistance for the CeCo-2 catalyst. The spectra were collected with an anodic polarization potential of 1.48 V vs RHE. The frequency range of EIS measurement were 0.01 to 10^6 Hz.

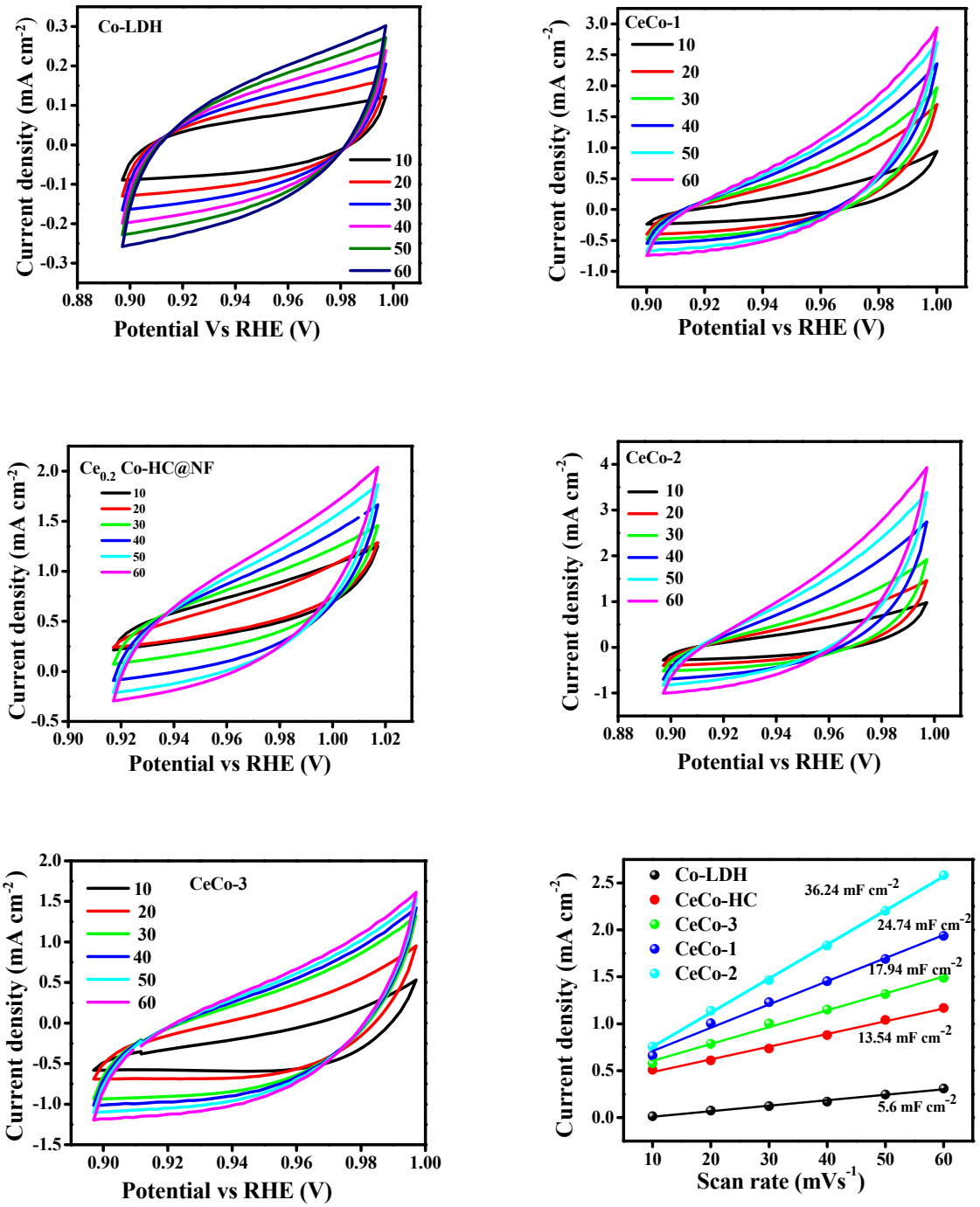

Figure S11. Determination of double-layer capacitance (C_{dl}) of Co-LDH, CeCo-1, CeCo-2, CeCo-3, by plotting (difference in current density)/2 against scan rate.

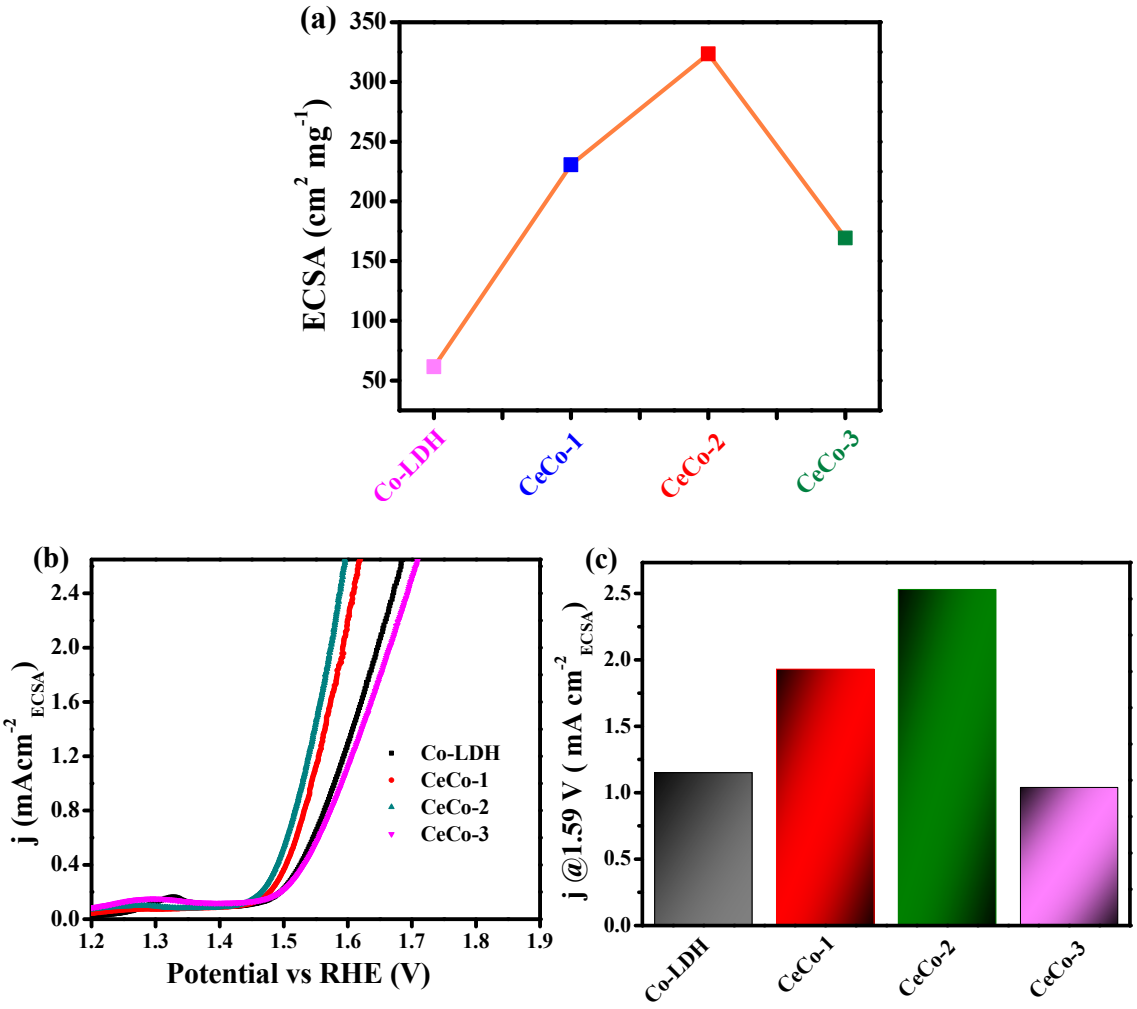

Figure S12. (a) ECSA of the catalysts showing the increase of ECSA with increasing amount of Ce, reached maxima for CeCo-2 and dropped with further increase in the amount of Ce(III). (b) ECSA normalized current density of the catalysts. (c) Plot for the ECSA normalized current density at 1.59 V showing the best activity for CeCo-2.

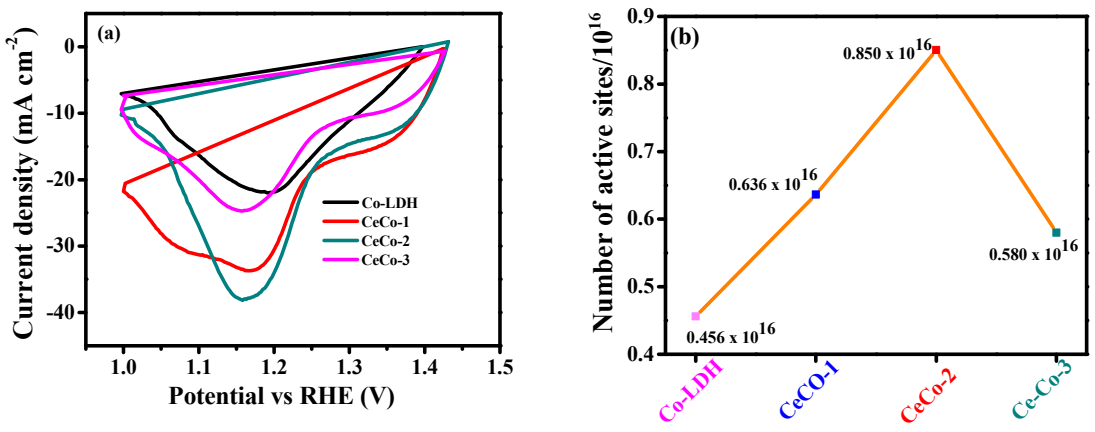

Figure S13. (a) Potential vs current density plots showing the reduction peak used for the area integration curve. (b) The number of active sites of the catalysts.

Determination of surface active sites using area integration of reduction peak [S22,S23]

The ECSA of a catalyst sample is calculated from the double-layer capacitance according to

ECSA = C_{dl}/C_s

C_s = 0.04 mF cm^{-2} in 1 M KOH based on typical reported values.

Where C_{dl} is the double layer capacitance of the catalyst and Cs is the specific capacitance of the material per unit area under identical electrolyte conditions.

For CeCo-2

Calculated area associated with the reduction peak = 6.802 x 10^{-6} V A

Hence the associated charge is = 6.802 x 10^{-6} V A / 0.005 V s^{-1}

= 1.36 x 10^{-3} A s

= 1.36 x 10^{-3} C

Now, the number of electron transferred is = 1.36 x 10^{-3} C / 1.602 ×10^{-19} C

= 0.850 x 10^{16}

Since the reduction of Co^{3+} to Co^{2+} is a single electron transfer reaction, the number of electrons calculated above is the same as the number of surface active sites.

Hence,

The surface-active site that participated in OER is = **0.850 x 10^{16}**

Calculation of Turn over frequency (TOF) of different catalysts [S22,S23]

TOF= (j × N_A) / (4 × F× n)

Where,

j = current density at η = 220 mV

N_A = Avogadro number

F = Faraday constant

n = number of active Co-sites

For CeCo-2

TOF = [(50 x 10^{-3}) x (6.023 x 10^{23})] / [(4) x (96485) x (0.850 x 10^{16})]

= 9.18 s^{-1}

Table S3. The determination of C_{dl} and ECSA for different catalysts.

S. No.	Catalyst	C_{dl} (mF cm^{-2})	ECSA (cm^2/mg)
1	Co- LDH	5.63	61.45
2	CeCo-1	24.74	230.7
3	CeCo-2	36.24	323.57
4	CeCo-3	17.94	169.24

Table S4. ECSA normalized OER activity of the reported catalysts compared with CeCo-2.

Entry	Catalysts	Potential (V) RHE	Current density (mA cm^{-2} ECSA)	Ref.
1	NiFe-LDH	1.58	0.1	S28
2	NiOOH	1.6523	10	S29
3	Co_9S_8/CoO/NC	1.5	0.009	S30
4	$Ni_{83}Fe_{17}$-ONCAS	1.568	1.0	S31
5	Ni–Fe NP	1.43	10	S32
6	Ni/MoO_2@CN	1.59	0.2	S33
7	NiFe-LDH	1.502	0.1	S34
8	$Ni(OH)_2$	1.603	0.1	S34
9	Ni_9FeOOH	1.45	0.028	S35
10	$Ir_{0.1}/Ni_9Fe$ SAC	1.45	0.053	S35
11	**CeCo-2**	**1.59**	**2.53**	**Our Work**

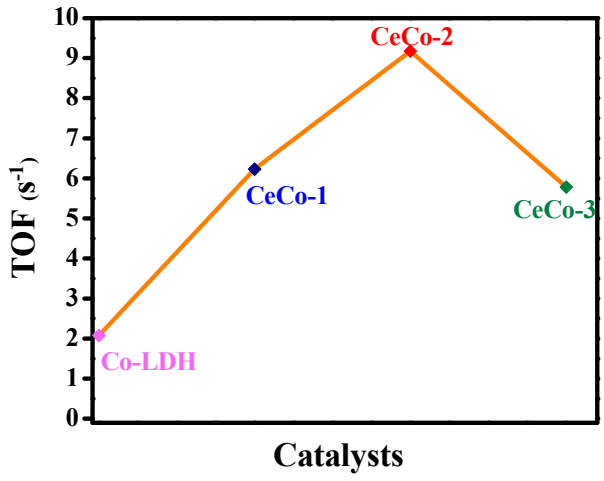

Figure S14. Plot of turnover frequency (TOF) of the catalysts.

Table S5. Number of active sites and TOFs of different catalysts.

S. No.	Catalyst	Area under the curve (VA)	No. of active sites	TOF (s^{-1})
1	Co-LDH	3.650×10^{-6}	0.451×10^{16}	2.05
2	CeCo-1	5.09×10^{-6}	0.636×10^{16}	6.237
3	**CeCo-2**	$\mathbf{6.802 \times 10^{-6}}$	$\mathbf{0.850 \times 10^{16}}$	**9.177**
4	CeCo-3	5.849×10^{-6}	0.580×10^{16}	5.785

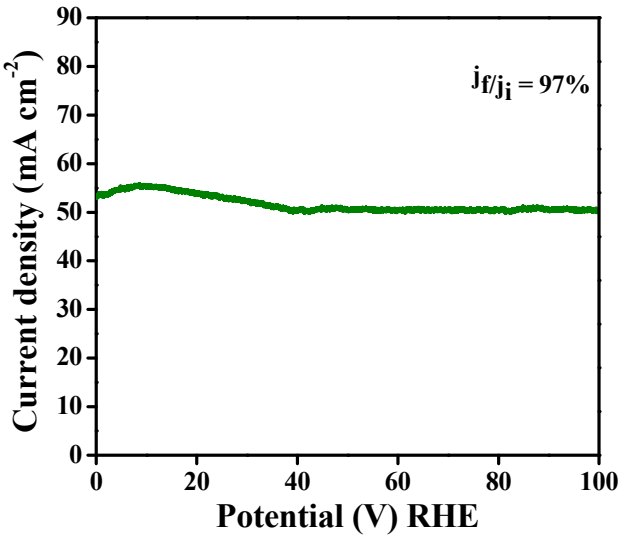

Figure S15. Long-term chronoamperometric OER with CeCo-2.

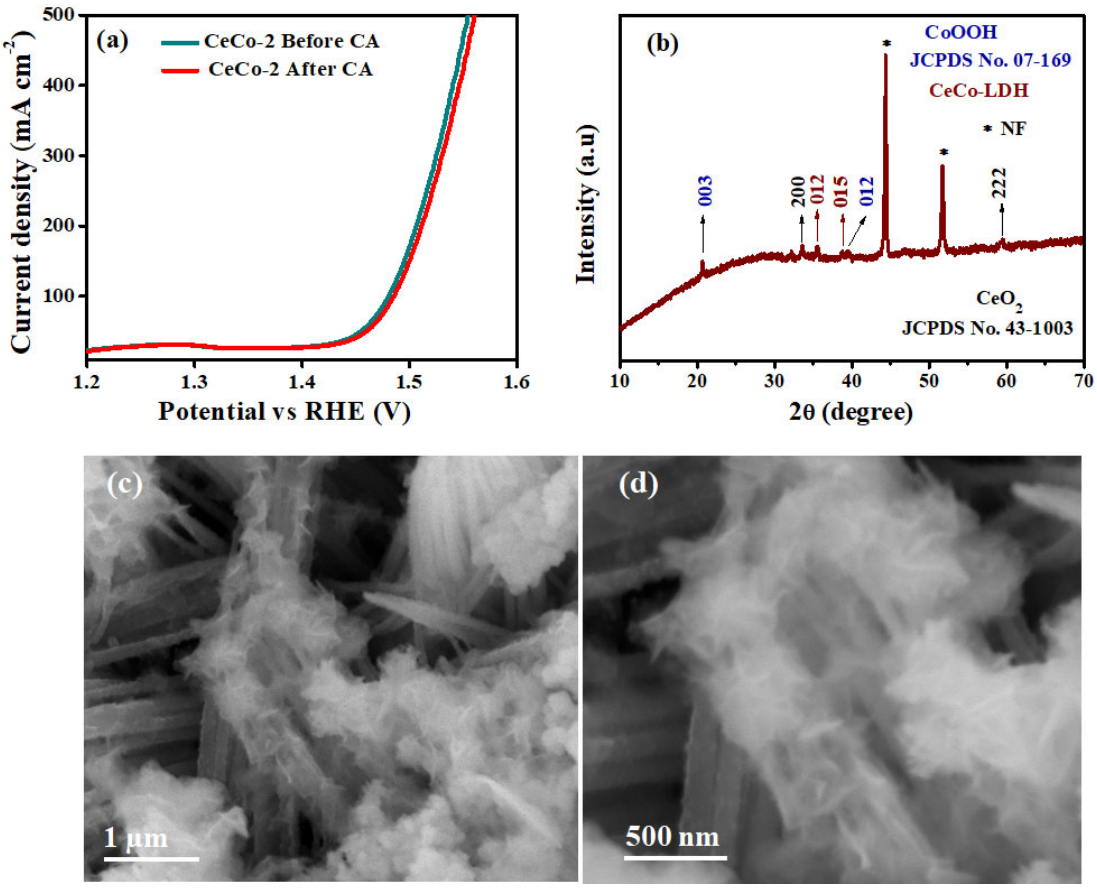

Figure S16. (a) LSV curves of CeCo-2 before and after CA, (b) PXRD of CeCo-2 after 100 h CA measurement, and (c-d) SEM images of CeCo-2 after 100 h CA measurement.

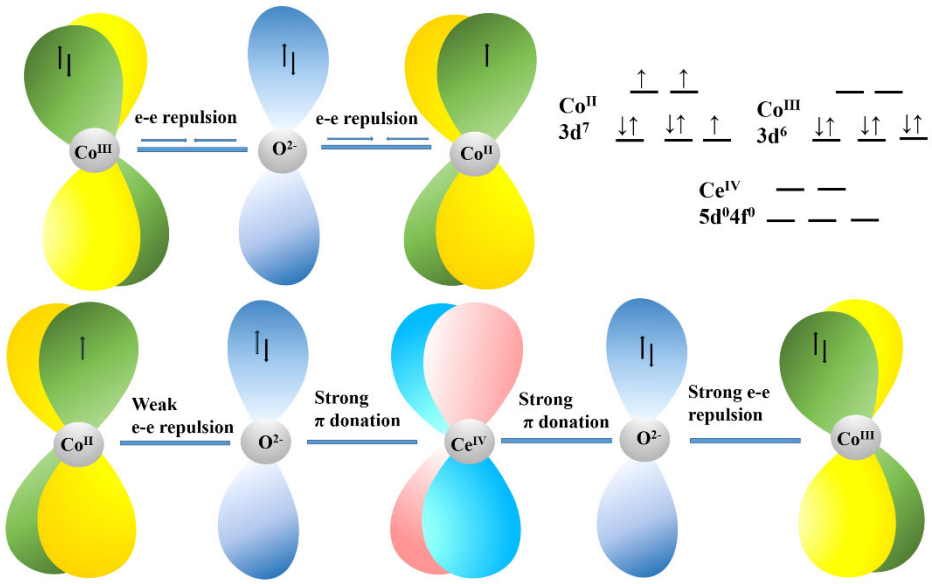

Figure S17. Schematic representation of π-orbital overlap to promote electron transfer from $Co^{II/III}$ to Ce^{IV} involving O (2p) π-orbital.

References

S1 H. Hu, B. Guan, B. Xia and X. W. Lou and *J. Am. Chem. Soc.*, 2015, **137**, 5590–5595.

S2 A. Indra, U. Paik and T. Song, *Angew. Chem. Int. Ed.*, 2018, **57**, 1241–1245.

S3 Z. Chen, Y. Ha, H. Jia, X. Yan, M. Chen, M. Liu and R. Wu, *Adv. Energy Mater.*, 2019, **9**, 1–13.

S4 Y. Lin, H. Wang, C. K. Peng, L. Bu, C. L. Chiang, K. Tian, Y. Zhao, J. Zhao, Y. G. Lin, J. M. Lee and L. Gao, *Small.*, 2020, **16**, 1–9.

S5 P. Maurya, V. Vyas, A. N. Singh and A. Indra, *Chem. Commun.*, 2023,**59**, 7200-720.

S6 Q. Dong, C. Shuai, Z. Mo, N. Liu, G. Liu, J. Wang, H. Pei, Q. Jia, W. Liu and X. Guo, *J. Solid State Chem.*, 2021, **296**, 121967.

S7 B. Singh and A. Indra, *Dalton Trans*., 2021, **50**, 2359-2363.

S8 Y. Hu, Z. Wang, W. Liu, L. Xu, M. Guan, Y. Huang, Y. Zhao, J. Bao, and H.-M. Li, *ACS Sustain. Chem. Eng.*, 2019, **7**, 16828-16834.

S9 T. Bhowmik**,** M. K. Kundu, and S. Barman**,** *ACS Appl. Energy Mater.*, 2018, **1**, 1200-1209.

S10 K. Bera, A. Karmakar, S. Kumaravel, S. S. Sankar, R. Madhu, H. N. Dhandapani, S. Nagappan, and S. Kundu, *Inorg. Chem.,* 2022, **61**, 4502-4512.

S11 L. Wen, X. Zhang, J. Liu, X. Li, C. Xing, X. L. W. Cai, W. Wang, and Y. Li, *Small*, 2019, **15**, 1902373.

S12 X. Yang, J. Cheng, Y. Xu, H. Li, W. Tu, and J. Zhou, *Chem. Eng. J*., 2023, ***472***,145076.

S13 S. Zhu, J. Wang, H. Li, J. Cai, Y. Li, J. Hu, Y. He, and Y. Zhou, *ACS Appl. Nano Mater.,* 2022, **5**, 13047.

S14 Y. Lin, H. Wang, C-K. Peng, L. Bu, C.-L. Chiang, K. Tian, Y. Zhao, J. Zhao, Y.-G. Lin, J.-M. Lee, and L. Gao, *Small.,* 2020, **16**, 2002426.

S15 J. X. Feng, S. H. Ye, H. Xu, Y. X. Tong and G. R. Li, *Adv. Mater.*, 2016, **28**, 4698–4703.

S16 M. C. Sung, G. H. Lee and D. W. Kim, *J. Alloys Compd.*, 2019, **800**, 450–455.

S17 D. Zhao, Y. Pi, Q. Shao, Y. Feng, Y. Zhang and X. Huang, *ACS Nano*, 2018, **12**, 6245–6251.

S18 Y. Liu, C. Ma, Q. Zhang, W. Wang, P. Pan, L. Gu, D. Xu, J. Bao and Z. Dai, *Adv. Mater.*, 2019, **31**, 1–9.

S19 M. Dinari, H. Allami and M. M. Momeni, *Energy and Fuels*, 2021, **35**, 1831–1841.

S20 M. Rong, H. Zhong, S. Wang, X. Ma and Z. Cao, *Colloids Surfaces. A: Physicochem. Eng. Asp.*, 2021, **625**, 126896.

S21 S. Xu, C. Lv, T. He, Z. Huang and C. Zhang, *J. Mater. Chem. A.*, 2019, **7**, 7526–7532.

S22 Y. R. Zheng, M. R. Gao, Q. Gao, H. H. Li, J. Xu, Z. Y. Wu and S. H. Yu, *Small*, 2015, **11**, 182–188.

S23 X. Du,Y. Ding and X. Zhang, *Appl. Surf. Sci.*, 2021, **562**,150227.

S24 H. Xu, B. Wang, C. Shan, P. Xi, W. Liu and Y. Tang, *ACS Appl. Mater. Interfaces*, 2018, **10**, 6336–6345.

S25 H. Xu, J. Cao, C. Shan, B. Wang, P. Xi, W. Liu and Y. Tang, *Angew. Chem. Int. Ed.*, 2018, **57**, 8654–8658.

S26 X. Wu, T. Zhang, J. Wei, P. Feng, X. Yan and Y. Tang, *Nano Res.*, 2020, **13**, 2130–2135.

S27 X. Yang, Z. Tao, Y. Wu, W. Lin and J. Zheng, *J. Alloys Compd.*, **2020**, 828, 154394.

S28 F. Dionigi, J. Zhu, Z. Zeng, T. Merzdorf, H. Sarodnik, M. Gliech, L. Pan, W-X. Li, J. Greeley and P. Strasser, *Angew. Chem. Int. Ed*., 2021, **60**, 14446– 14457.

S29 S. Ananthraj and S. Kundu, *ACS Energy Lett.*, 2019, **4**, 1260−1264.

S30 K. U. Rahman, S. Airam, X. Lin, J. Gao, Q. Guo and Z. Zhang, *Nanomater*., 2021, **11**, 2237.

S31 P. Liu, B.C. Chen, C. Liang, W. Yao, Y. Cui, S. Hu, P. Zou, H. Zhang, H. J. Fan and C. Yang, *Adv. Mater*. 2021, **33**, 2007377.

S32 B. H. R. Suryanto, Y. Wang, R. K. Hocking, W. Adomson and C. Zhao, *Nat. Commun*., 2019, **1**, 5599.

S33 G. Qian, J. Chen, T. Yu, J. Liu, L. Luo and S. Yin, *Nano-Micro Lett*., 2022, **14**, 1-15.

S34 S. S, Jeon, P. W. Kang, M. Klingenhof, H. Lee, F. Dionigi and P. Strasser, *ACS Catal*., 2023, **13**, 1186−1196.

S35 X. Zhenga, J. Tanga, A. Galloc, J. A. G, Torresc, X. Yua, C. J. Athanitisa, E. M, Beena, P. Erciusd, H. Maoe, S. C. Fakraf, C. Songd, R. C. Davisg, J. A. Reimere, J. Vinsonh, M. Bajdichc and Y. Cuia, *PNAS*., 2021, **118**, e2101817118.